Research Article Vol. 57, No. 29 / 10 October 2018 / Applied Optics 8743

applied optics

Temperature-dependent terahertz spectroscopy and refractive index measurements of aqua-soluble and plastic explosives

Ganesh Damarla,[1] M. Venkatesh,[1,2] and A. K. Chaudhary[1,*]

[1]Advanced Centre of Research in High Energy Materials (ACRHEM), University of Hyderabad, Hyderabad 500046, Telangana, India
[2]The Guo China-US Photonics Laboratory, State Key Laboratory of Applied Optics, Changchun Institute of Optics, Fine Mechanics and Physics, Chinese Academy of Sciences, Changchun 130033, China
*Corresponding author: anilphys@yahoo.com

Received 9 July 2018; revised 8 September 2018; accepted 11 September 2018; posted 11 September 2018 (Doc. ID 335656); published 10 October 2018

The paper reports the temperature-dependent time domain terahertz spectroscopy of premium aqua-soluble and plastic explosives such as NH_4NO_3, TNT, and RDX between 0.1 and 2.2 THz. Tunable terahertz radiation was generated using ZnTe crystal as a source, and a photoconductive antenna was used as a detector. The temperature-dependent study was carried out between 30°C and 200°C in a specially designed oven. The signature peaks of RDX and TNT present at 0.82 and 1.60 THz, respectively, show a strong redshift, whereas the NH_4NO_3 molecule shows a comparatively small shift. The high-temperature-based redshift phenomenon is just the opposite of the blueshift recorded at low temperatures. In addition, the temperature-dependent absorption coefficient data of these molecules support the change in the concentration of the NO_2 molecule. We have also ascertained the temperature-dependent refractive indices of these molecules between 0.1 and 2.0 THz, which confirms the effect of temperature on the refractive indices. Finally, the signature peak of RDX with respect to the reduction in the weight concentration of RDX in the Teflon matrix was studied at 0.82 THz.

https://doi.org/10.1364/AO.57.008743

1. INTRODUCTION

Terahertz (THz) radiation has low energy and deep penetration ability when applied to leather, cloth, Teflon (PTFE) and packing materials [1,2]. Therefore, it is treated as a nondestructive and noninvasive tool for the analysis of explosives, drugs, and biomolecules [3]. Moreover, it covers the fingerprint region of the vibrational–rotational lines of most of the organic, inorganic and biological molecules. Recently, THz technology-clubbed materials have been used for sensing and medical diagnostic applications, such as graphene-based sensors and meta devices based on conductivity changes and refractive index in the THz regime [4–8]. NH_4NO_3, a well-known aqua-soluble fertilizer that is an inorganic molecule, is used as a principal ingredient in improvised explosive devices and presents a major challenge in detection by means of existing optical techniques. Similarly, RDX and TNT are crystalline and amorphous aromatic organic compounds. TNT is partially soluble in water, while RDX is soluble only in organic solvents. Therefore, TNT is responsible for contamination of underground water near military testing ranges. However, RDX is one of the most powerful plastic explosives. It is shock-insensitive and insoluble in water and finds potential use in industry and defense [9].

Tunable THz radiation between the 0.1 and 3 THz range can be generated using different types of optical techniques using low-temperature and semi-insulating GaAs-based photoconductive antennas and nonlinear crystals such as ZnTe, 4-N-methylstilbazolium tosylate (DAST), and N-benzyl-2-methyl-4-nitroaniline (BNA) [10–13]. The THz radiation generated is employed to record the time domain spectra of solid explosives in pellet form. The premier explosive materials have sharp spectral features above 3 THz. The detection and identification of explosives in concealed conditions in field applications are challenging and require judicious selection of the THz frequency range. The high-energy materials (HEMs) RDX and NH_4NO_3 are crystalline, whereas TNT is amorphous in nature. Khachatrian *et al.* have reported the sharp rotational–vibrational features of NH_4NO_3 at low temperatures using a metallic substrate [14]. However, NH_4NO_3 powder mixed with PTFE powder in specific proportions provides information about some distinguishing sharp vibrational modes in transmission range. Most of the solid granule samples dimensions are comparable with the wavelength of THz radiation, which enhances the scattering losses [15]. Therefore, it experiences technical difficulty in direct recording of their spectra.

Chen *et al.* reported some distinguishing weak spectral features of NH_4NO_3 between 0.1 and 3 THz at ambient temperature [16]. Hu *et al.* reported on the THz time domain spectroscopy of explosives [17]. However, most of the reported studies have not incorporated the high-temperature spectra of HEMs. These materials are used in rocket fuel, and the study of thermal decomposition mechanisms provides important information about the energy release process. In the THz domain it is also important to know the participation of different intact functional groups at the time of heating. In our earlier work we carried out this study in vapor form between 40°C and 350°C using a UV–visible wavelength based pulsed photoacoustic technique [18–21]. In the present work we have recorded the spectral signatures of HEMs, and our results have found good agreement with reported values. In addition, we have demonstrated the hot band vibration spectra of the solid explosives NH_4NO_3, RDX, and TNT. The main problem in recording THz spectra in air is related to the presence of water molecules, which have strong absorption peaks in the THz domain and also overlap some of the signature peaks of the samples [22]. But gradual heating of the sample initiates the process of vaporization. Consequently, the intensity of the water absorption band decreases with the increase in temperature. In addition, our studies clearly confirm the release of NO_2 molecules just above 40°C, which also supports our previous studies on the number of explosive molecules. The study was based on the recording of strong vibronic transitions of NO_2 molecules between 30°C and 350°C using a pulsed photoacoustic technique. Here we have also made an attempt to develop a small quantity of pellets using PTFE powder at room temperature and have successfully recorded their characteristic signature in the THz domain.

2. EXPERIMENT DETAILS

The experiment was carried out in two steps. In the first step, we prepared the explosive pellets in the PTFE matrix, and in the second step, these pellets were subjected to the THz system for the recording of temperature-dependent time domain spectra. Sample preparation is an important factor for the recording of a characteristic signature [21,23]. A pure sample in powder form was mixed with PTFE powder, which has very low absorption in the THz range. An explosive sample weighing around 200 mg was mixed with 800 mg of PTFE powder using 10 ml of CH_3OH solvent. The mixture was dried for 20 min and then ground with a mortar to produce a fine homogenous powder. The powder mixture was divided into two halves and transferred to the die using butter paper, and then was pressed with 2 tons of pressure to prepare a pellet. The thickness and diameter of the pellets are ∼2 mm and 12 mm, respectively. The THz wavelength matches the size of the sample present in the pellets, which is responsible for the inhomogeneous broadening of the spectral peaks due to the scattering effect. Moreover, scattering in THz spectra is caused by the refractive index mismatch between the sample crystals and the surrounding pellet medium (PTFE in this case). However, the effect of scattering due to the multiple crystalline nature of the samples can be overcome by dissolving the mixture in methanol solution. We also mixed different proportions of the RDX sample in the PTFE matrix to record the weight-percentage-based signature peaks.

A Ti:sapphire femtosecond oscillator (Coherent Chameleon Ultra II) was used as a laser source. It delivers *p*-polarized laser pulses of 140 fs duration at a 80 MHz repetition rate. The laser output wavelength was tuned between 780 and 850 nm for THz generation. The variable attenuator (VA; Eskpla) was employed to attenuate the output average power. The incident average power was allowed to be incident on the 110 cut ZnTe crystal of 2.0 mm thickness for THz generation. The crystal was housed in a PTFE holder and placed in an optical rotator for vertical rotation. The incident femtosecond laser pulses were loosely focused onto the crystal by means of a plano-convex lens L_1 with a focal length 30 cm. The spot diameter of the laser pulse on the ZnTe crystal was ∼234 μm. The generated THz radiation was collected using two off-axis parabolic mirrors (PM_1, PM_2). The diameter (D) and effective focal length (f_e) of the parabolic mirrors (Thorlabs MPD508762-90-M01) were ∼50 mm and ∼150 mm, respectively. The residual transmitted laser pulses from the source were separated from the THz radiation using a high-resistivity float zone silicon plate (diameter 50 mm, thickness 2 mm) and black polyethylene filter. The silicon plate has reflection coating in between 700 and 900 nm laser wavelengths. The diverging THz radiation emitted from the source was collimated and focused by mirrors PM_1 and PM_2. PM_2 focused the generated the THz radiation onto the photoconductive antenna, which was coupled with the preamplifier, and the output of the preamplifier was fed to the lock-in amplifier. The output signal from the lock-in amplifier was sent to the computer for the recording of time and frequency domain signals using an indigenously designed data acquisition program made using LabVIEW. The horizontal dynamic range of the spectrometer was limited up to 2.2 THz. The pure PTFE pellet was used as a reference. It was assumed that the explosive sample was homogeneously distributed in the PTFE matrix. Barber *et al.* reported temperature-dependent THz spectroscopy of explosives between 8 K and 300 K [24]. However, in the present report we have carried out the high-temperature study of explosive samples below their melting point to record the change in the absorption characteristics and refractive indices. The sample pellet was placed between the parabolic mirrors for the recording of the time domain spectrum, as shown in Fig. 1.

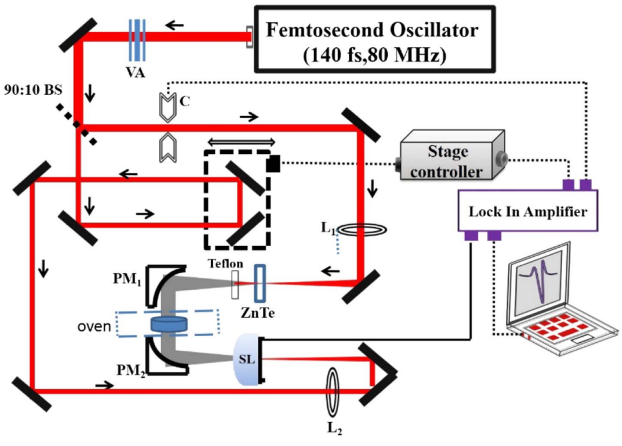

Fig. 1. Schematic layout of a THz time domain spectrometer.

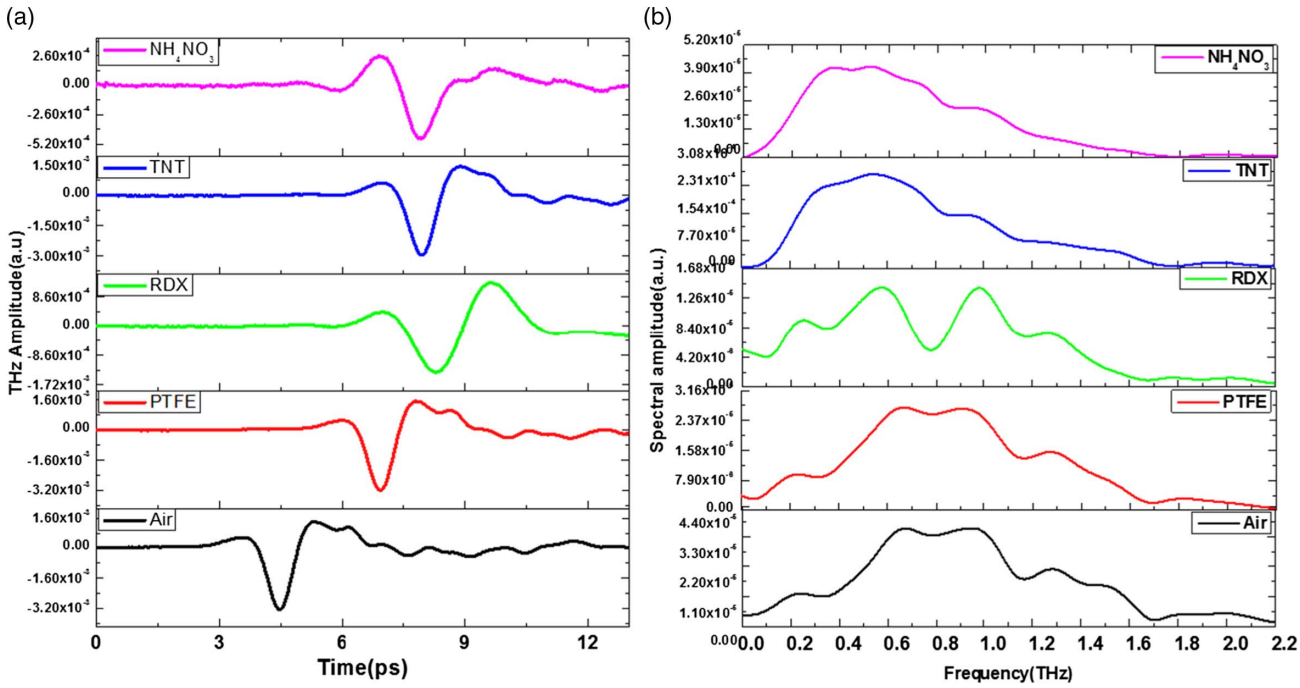

Fig. 2. Schematic THs spectrum. (a) Temporal profile of THz pulse, (b) frequency domain spectra of different explosives.

The average incident power of the THz falling on the sample pellet was of the order of 700 μW. Abid *et al.* [25] reported using optical-extinction-model-based plasmon–exciton interactions between 115 K and 295 K to generate energy of the order of 42 meV, which is equivalent to 10 THz. The authors used a Ti:sapphire laser source tunable between 750–850 nm wavelength for this purpose. However, we generated a THz radiation acceptable region at room temperature using an 800 nm wavelength. The generated broadband THz radiation spectra lies between 0.4 and 8.27 meV. The THz absorption spectroscopy of explosive molecules was carried out in a specially designed small-sized oven that can accommodate the pellets inserted between two parabolic mirrors. The oven works on the Peltier heating principle and was supplied by Conversion Co. Ltd. (UK). We redesigned the hood of the oven to accommodate an explosive pellet with a 12 mm diameter. The temperature of the oven was controlled between 25°C and 200°C with a precision of +0.01°C using a temperature controller supplied by the same company.

3. THEORY

The time domain THz signal received after passing through the samples was converted into a frequency domain spectrum using fast Fourier transform (FFT). The value of the absorption coefficient $\alpha(\omega)$ was calculated from the FFT spectrum. The transmitted field T is given by

$$T = \frac{E_{\text{sample}}}{E_{\text{Reference}}}, \tag{1}$$

where E_{sample} and $E_{\text{Reference}}$ are the amplitudes of the THz radiation after passing through the material and reference samples, respectively. We can calculate the effective thickness (l) of the sample distributed in the PTFE matrix using the formula

$$l = \frac{m}{\rho}\frac{4}{\Pi D^2}. \tag{2}$$

Here, m is the weight of the sample (100 mg), D is the diameter of the sample (12 mm), and ρ is the density of the sample. Since the pellet contains a mixture of two samples, the absorption coefficient α can be ascertained using the formula [26,27]

$$\text{Absorption coefficient}(\alpha) = -\frac{1}{l}\ln\frac{T_m}{T_R}, \tag{3}$$

where l is the effective thickness of the sample and T_m and T_R are transmitted THz amplitudes from the samples and the reference, respectively. The refractive index of the sample can be calculated by using the formula [28]

$$n = 1 + \frac{\Delta\phi \times c}{2\pi\nu \times d}, \tag{4}$$

where $\Delta\phi$ is the phase difference between the reference and the sample, ν is the frequency, d is the thickness of the pellet, and c is the velocity of light. The complex refractive index is represented using the Kramers–Kronig model,

$$n = n + i\kappa, \tag{5}$$

where n is the real part of the refractive index and κ is the extinction coefficient. κ is related to the power absorption coefficient α.

4. RESULTS AND DISCUSSION

Figures 2(a) and 2(b) show the temporal and frequency domain spectral profiles of air, PTFE, and the explosives in the THz range after passing through the pellet. It is observed that the THz pulse shows variations in delay time after passing through different explosives range. It is attributed to the change in the optical path length of the radiation, which varies from sample

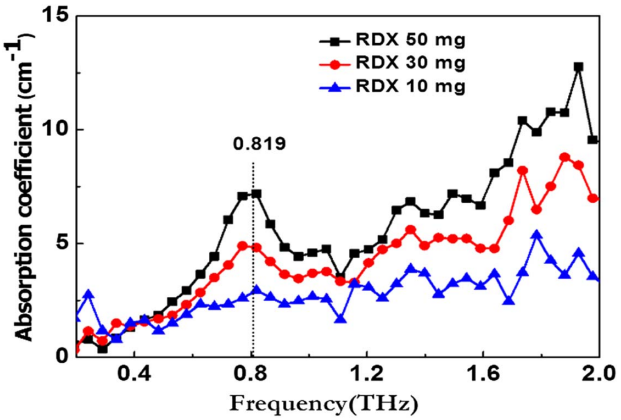

Fig. 3. Absorption coefficients of RDX for different weight concentrations.

to sample due to the change in the refractive index of the molecules. The spectral intensity clearly shows the variation in the intensity and the shift in the absorption peaks of explosive molecules. The experiment was performed in ambient room temperature.

Figure 2 depicts the temporal and frequency domain spectra of explosive samples between 0.1 and 2.0 THz. The dynamic range of the amplitude of spectral lines lies between 10^{-4} and 10^{-7} on a log scale, which helps us to record the weak absorption peaks of the explosive molecules. It is clear that the water-soluble compound NH_4NO_3 has a high absorption coefficient compared to the aqua-insoluble explosives [16]. However, RDX has a significant characteristic absorption peak at 0.82 THz, which agrees with reported work [29,30]. All the samples show a common feature near 1.8 THz. The absorption peak is attributed to the intermolecular vibrational modes present in the THz region. The corresponding THz absorption peaks for NH_4NO_3 present at 98.15, 108.5, and 143.7 cm^{-1} are 0.87, 1.5, and 1.81 THz, respectively.

All the abovementioned studies were carried out with 100 mg of explosive sample mixed with 400 mg of PTFE matrix. We also made an attempt to study the effect of weight percentage on the signature peak of the explosive sample. Therefore, pellets with different weight concentrations of RDX such as 50, 30, and 10 mg were prepared in the PTFE matrix. The thickness and size of the pellets were controlled by adding the same weight percentage of PTFE powder into the mixture. As a result, the total weight of the pellet matrix always remains 500 mg. The time domain spectra of different weight percentage pellets were recorded, and their corresponding absorption coefficient data were ascertained and compared with the reported values available in the literature [31,32].

Figure 3 shows the drop in the value of the absorption coefficient with a decreasing concentration of RDX in PTFE matrix at 0.81 THz. This also indicates the minimum detection limit of RDX in solid form.

A. Temperature-Dependent Absorption Spectra and Refractive Index of RDX

The recording of absorption bands in the THz region is also affected by the presence of water vapor. Consequently, many of the characteristic bands are either not visible or have low intensity. The temperature-dependent spectroscopy of molecules plays a very important role in revealing significant information about many weak vibrational modes that are not observable at room temperature [33,34]. In addition, it helps excite the molecules at the ground state, which is also reflected in the coupling of oscillating modes in terms of redshift. In this section we discuss the temperature-dependent THz spectra of RDX, TNT, and NH_4NO_3 molecules in solid form. The spectra are recorded below their melting point.

Shen *et al.* [34], Hangyo *et al.* [35], and Azad *et al.* [36] reported the temperature-dependent spectroscopic study at low temperature and identified the behavior of signature peaks of RDX present at 0.82, 1.05, 1.50, and 1.96 THz. Figure 4(a) shows the temperature-dependent absorption coefficients of RDX in PTFE matrix recorded between 30°C and 170°C. The characteristic band present at 0.8 THz has sharp features between 30°C and 90°C. This can be attributed to the presence of the NO_2 group [37]. The absorption coefficient at room temperature is 11 cm^{-1}, which decreases with increasing sample temperature. In addition, the shape of the absorption peak between 30°C and 90°C shows a broadening effect at 105°C. This reveals the process of vaporization of water molecules and the release of NO_2 gas, which also indicates the initiation of the process of thermal decomposition of RDX. The decrease in the

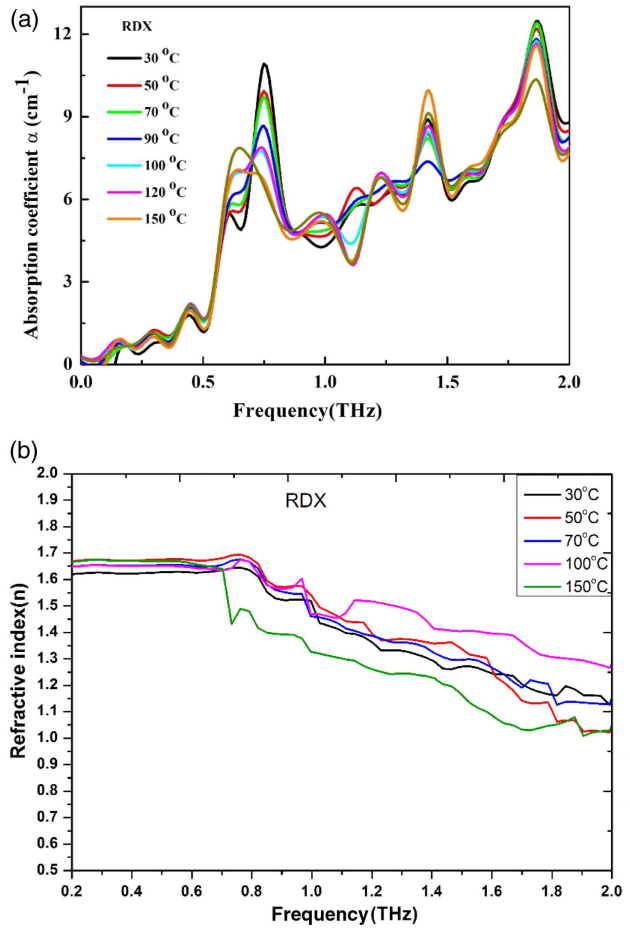

Fig. 4. (a) Temperature-dependent absorption coefficient of RDX, (b) temperature-dependent refractive index of RDX.

absorption coefficient value of the 0.8 THz peak is directly linked to the loss of NO_2 from the solid sample [38]. In our previous reports, we have successfully demonstrated the release of NO_2 from different explosives above 40°C, using a pulsed photoacoustic technique [28,39,40]. The previous study was performed in vapor using 532 and 266 nm wavelengths of a *Q*-switched Nd:YAG laser. The NO_2 gas release mechanism is based on the strong electronic transition and is attributed to vibronic modes of NO_2. However, the present results once again support our earlier findings in the THz domain. Further, an increase in the temperature between 120°C and 170°C enhances the broadening of the peak width and shows some shift toward 0.62 THz, which is nothing but the redshift effect due to heating. Similarly, the peak at 1.05 THz has a small amplitude and appears in the form of a dip at room temperature. However, after crossing 105°C, the dip is modified and converted into a hump at 120°C. This is attributed to the hot band effect, where the weak signature peak was invisible due to water molecules. A similar type of effect is also observed at 1.4 THz. However, this peak shows the reverse trend. The absorption coefficient between 30°C and 105°C is lower than the absorption coefficient at 150°C.

Figure 4(b) shows the temperature-dependent refractive index of RDX. The refractive index was recorded between 30°C and 150°C, and it is clear that there is little variation in the refractive index up to 0.7 THz. The value of the refractive index remains between 1.6 and 1.65. However, after 0.7 THz there is a large decline in the value of the refractive index with respect to temperature, and it decreases from 1.7 to 1.2 at 2.0 THz. Similar types of changes are also visible in the absorption coefficient data at 0.7 THz.

B. Temperature-Dependent Absorption Spectra and Refractive Index of TNT

Figure 5(a) shows the temperature-dependent spectrum of TNT, which was recorded between 30°C and 70°C—below its melting point, i.e., 80.35°C. For TNT, characteristic absorption peaks are present at 1.6 THz and 2.17 THz [39]. One can easily see that the peak at 30°C has a higher absorption coefficient around 7.4 cm^{-1} and decreases to 6 cm^{-1} at 50°C and almost becomes 4.85 at 70°C. After crossing this temperature, the peak shows an unusual reverse trend. It also indicates the process of initiation of a slow release of NO_2 from the solid sample. Similarly, the absorption coefficent of the 2.17 THz peak is 10.65 cm^{-1}, which becomes 7.8 cm^{-1} at 50°C and 6.62 cm^{-1} at 70°C. The decreasing trend of the absorption coefficient with respect to temperature also appears in the form of a redshift toward the left side at 70°C. This redshift effect is due to a hot band transition peak at 2.2 THz, which has a higher value at 30°C. Therefore, the temperature-based recording of signature peaks clearly reflects the process of thermal loss of TNT molecules at high temperatures. In addition, temperature-based spectroscopy confirms the presence of some prominent signature peaks in a repeated manner, along with redshift. Two signature peaks located at 1.77 and 2.17 THz at 30°C get shifted to 1.722 and 2.097 THz at 70°C, respectively.

Figure 5(b) shows the temperature-dependent refractive index of TNT. The refractive index was recorded between 30°C and 70°C, and it is clear that there is very little variation in the refractive index up to 1.6 THz. The value of the refractive index between 30°C and 70°C almost overlaps and remains between 1.55 and 1.60. However, after 1.6 THz it shows great variation between 1.55 and 1.75. Similar types of changes are also visible in absorption coefficient data at 1.6 THz.

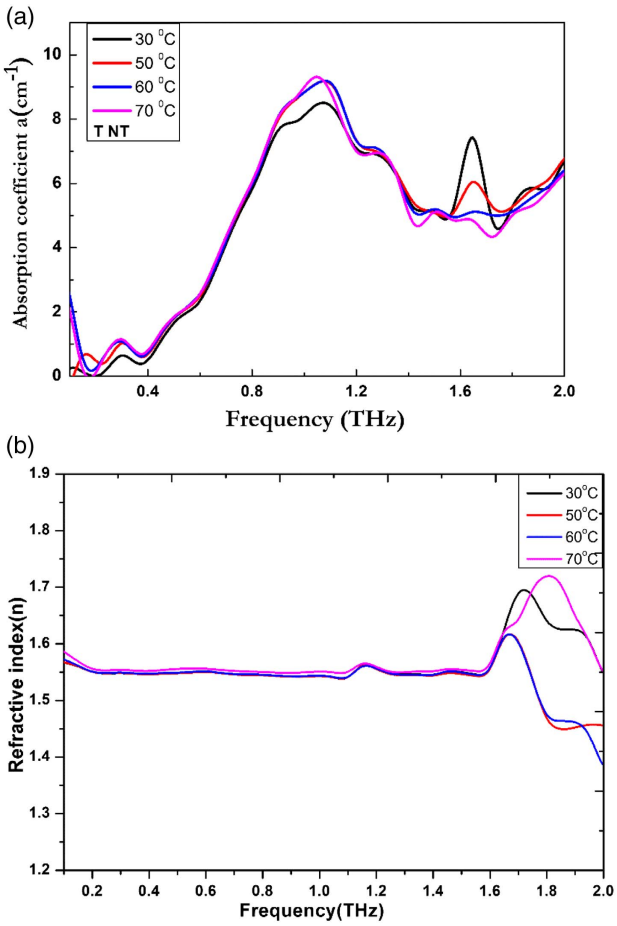

Fig. 5. (a) Temperature-dependent absorption coefficient of TNT, (b) temperature-dependent refractive index of TNT.

C. Temperature-Dependent Absorption Spectra and Refractive Index of NH_4NO_3

Figure 6(a) shows the temperature-dependent absorption spectra of NH_4NO_3. The frequency spectra clearly show the presence of a weak signature at room temperature. An earlier reported study of NH_4NO_3 was carried out at low temperature and demonstrated the conversion of the absorption peak into a kink at 1.7 THz [28,41,42]. However, when NH_4NO_3 is mixed with PTFE, it starts showing a strong signature even at room temperature. The absorption peaks at 1.2 and 1.4 THz are weaker than the peak at 1.78. It also shows a maximum intensity peak at 105°C below the melting point of NH_4NO_3.

Figure 6(a) shows the absorption spectrum of NH_4HO_3 recorded between 30°C and 150°C at 0.1–2.0 THz. To the best of our knowledge, it is the first demonstration of a signature peak of NH_4HO_3 at 1.73 THz. At room temperature, i.e., 30°C, it has an absorption coefficient of the order of 5.69 cm^{-1}. Since the spectra are recorded in transmission mode, these signature peaks are visible. Further, the effect of a redshift is also

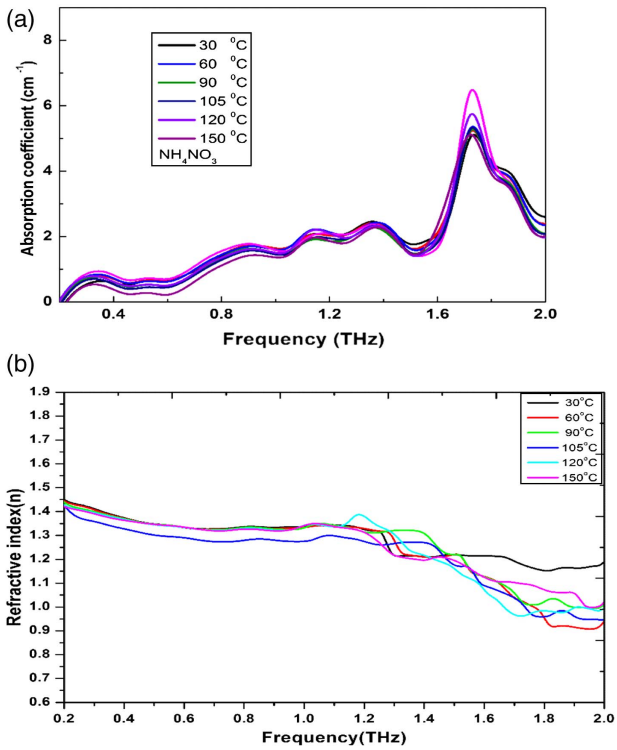

Fig. 6. (a) Temperature-dependent absorption coefficient of NH_4NO_3, (b) temperature-dependent refractive index of NH_4NO_3.

visible at 1.78 THz. The value of the absorption coefficient is of the order of 5.27 cm^{-1} between 60°C and 90°C. It is further shifted toward 1.722 THz with a corresponding absorption coefficient of 5.05 cm^{-1} between 120°C and 150°C, respectively. The NH_4NO_3 is a very stable inorganic aqua molecule due to ionic bonds. Therefore, it does not show a similar type of decomposition behavior and strong absorption like RDX and TNT [43]. As a result, the redshift effect is not very prominent.

Figure 6(b) shows the temperature-dependent refractive index of NH_4NO_3. The refractive index is recorded between 30°C and 150°C, and it is clear that little variation exists in the refractive index up to 1.3 THz. The value of the refractive index remains between 1.42 and 1.40. However, after 1.3 THz the value of the refractive index shows a fall with respect to temperature and decreases from 1.4 to 1.0. Similar types of changes are also visible in the absorption coefficient data at 1.3 and 1.6 THz.

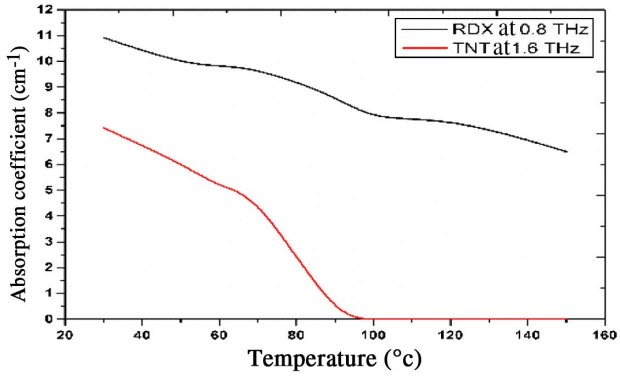

Fig. 7. Variation of absorption coefficients of RDX and TNT with temperature.

Table 1. Absorption Coefficient, Signal Sensitivity, and Sample Thickness Data for the Different Samples

Sample Pellet Name	Thickness of Pellet (mm)	THz Peak Value (a.u.)	Absorption Coefficient (cm^{-1}) at Room Temperature
RDX	1.91	1.83×10^{-4}	11.2
TNT	1.97	3.4×10^{-4}	9.98
NH_4NO_3	2.1	1.73×10^{-5}	5.67

Figure 7 shows the variation in the values of the absorption coefficients of characteristic peaks of RDX and TNT with respect to temperature. Since RDX is more stable and stronger than TNT, the loss of NO_2 takes place in multiple steps. This is also reflected in the upper curve, where the value of the absorption coefficient falls gradually from 11 to 7.7 cm^{-1}, whereas TNT shows a direct fall from 7.5 to 0 cm^{-1} after crossing the melting point.

5. SENSITIVITY AND LIMITATIONS

We have compiled the sample thickness, signal sensitivity, and absorption coefficient data of the three explosives in Table 1.

La Spada and Vegni studied a metamaterial-based wideband electromagnetic wave absorber with normal incidence and thickness dependency and reported notch action at 185 THz with normal incidence [5]. In our case it is evident from the table that the absorption coefficient is completely material dependent and more for RDX. We detected 10 mg of RDX in PTFE matrix, which shows a 5 cm^{-1} absorption coefficient value. Further improvisation is needed to reduce the quantity of the sample. In the present experiment, the THz beam spot size is 6 mm, and we require a pellet with a minimum size of 8.0 mm. Therefore, we are required to select suitable parabolic mirrors to reduce the spot size of the order of 2.0 mm, which will also help reduce the pellet diameter of the order of 2.0 mm and enhance the detection sensitivity. Similarly, the temperature-based study also helped to elucidate the redshift behavior of explosive molecules, which varies from sample to sample. Finally, a temperature-dependent theoretical model needs to be developed to explain the vibronic and rotational transition behavior of these molecules in the THz region, as existing density functional theory calculations are based at 0 K.

6. CONCLUSIONS

We have successfully recorded the temperature-dependent refractive indices and absorption coefficients of NH_4NO_3, TNT, and RDX explosives below their melting points. Also, we demonstrated the temperature-dependent redshift effect in these molecules. To the best of our knowledge, this is the first demonstration of the redshift effect and the process of slow thermal decomposition mechanisms of these explosives in the THz domain. This also helps characterize the explosive molecules. In addition, the changes in the strength of the THz signal of RDX in PTFE matrix are related to the concentration.

Funding. Defence Research and Development Organisation (DRDO), Ministry of Defence, and Govt. of India (ERIP/ER/1501138/M/01/319/D(RD)).

Acknowledgment. The authors thank the director of HEMRL, Pune, for providing pure explosive samples and the director of ACRHEM for constant support and encouragement during the experiment. Thanks are also due to Apar Industries Ltd. (Khattalwada, Umbargaon, Dist. Valsad, Gujrat-396120) for providing the high-grade PTFE (Teflon) powder used in the experiment.

REFERENCES

1. M. Tonouchi, "Cutting-edge terahertz technology," Nat. Photonics **1**, 97–105 (2007).
2. D. J. Funk, F. Calgaro, R. D. Averitt, M. L. T. Asaki, and A. J. Taylor, "THz transmission spectroscopy and imaging: application to the energetic materials PBX 9501 and PBX 9502," Appl. Spectrosc. **58**, 428–431 (2004).
3. J. A. Zeitler, K. Kogermann, J. Rantanen, T. Rades, P. F. Taday, M. Pepper, J. Aaltonen, and C. J. Strachan, "Drug hydrate systems and dehydration processes studied by terahertz pulsed spectroscopy," Int. J. Pharm. **334**, 78–84 (2007).
4. A. Vakil and N. Engheta, "Transformation optics using graphene," Science **332**, 1291–1294 (2011).
5. L. La Spada and L. Vegni, "Electromagnetic nanoparticles for sensing and medical diagnostic applications," Materials **11**, 603 (2018).
6. N. I. Zheludev and Y. S. Kivshar, "From metamaterials to metadevices," Nat. Mater. **11**, 917–924 (2012).
7. L. La Spada and L. Vegni, "Near-zero-index wires," Opt. Express **25**, 23699–23708 (2017).
8. Y. Lee, S.-J. Kim, H. Park, and B. Lee, "Metamaterials and metasurfaces for sensor applications," Sensors **17**, 1726 (2017).
9. A. G. Davies, A. D. Burnett, W. Fan, E. H. Linfield, and J. E. Cunningham, "Terahertz spectroscopy of explosives and drugs," Mater. Today **11**(3), 18–26 (2008).
10. M. Venkatesh, K. S. Rao, T. S. Abhilash, S. P. Tewari, and A. K. Chaudhary, "Optical characterization of GaAs photoconductive antennas for efficient generation and detection of terahertz radiation," Opt. Mater. **36**, 596–601 (2014).
11. K. S. Rao, A. K. Chaudhary, M. Venkatesh, K. Thirupugalmani, and S. Brahadeeswaran, "DAST crystal based terahertz generation and recording of time resolved photoacoustic spectra of N2O gas at 0.5 and 1.5 THz bands," Curr. Appl. Phys. **16**, 777–783 (2016).
12. M. Venkatesh, K. Thirupugalmani, K. S. Rao, S. Brahadeeswaran, and A. K. Chaudhary, "Generation of efficient THz radiation by optical rectification in DAST crystal using tunable femtosecond laser pulses," Indian J. Phys. **91**, 319–326 (2017).
13. P. Jepsen and B. Fischer, "Dynamic range in terahertz time-domain transmission and reflection spectroscopy," Opt. Lett. **30**, 29–31 (2005).
14. A. Khachatrian, S. Qadri, and J. S. Melinger, "High resolution THz spectroscopy of ammonium nitrate and potassium nitrate crystalline films," in *International Conference on Infrared, Millimeter, and Terahertz Waves* (2011).
15. T. Bardon, R. K. May, P. F. Taday, and M. Strlič, "Influence of particle size on optical constants from pellets measured with terahertz pulsed spectroscopy," IEEE Trans. Terahertz Sci. Technol. **6**, 408–413 (2016).
16. J. Chen, Y. Chen, H. Zhao, G. J. Bastiaans, and X.-C. Zhang, "Absorption coefficients of selected explosives and related compounds in the range of 0.1–2.8 THz," Opt. Express **15**, 12060–12067 (2007).
17. Y. Hu, P. Huang, L. Guo, X. Wang, and C. Zhang, "Terahertz spectroscopic investigations of explosives," Phys. Lett. A **359**, 728–732 (2006).
18. A. K. Chaudhary, K. S. Rao, and A. Sudheer Kumar, "Study of thermal decomposition mechanisms and absorption cross section of nitro-rich phenyl- and bis-series 1, 2, 3-triazoles," Appl. Opt. **55**, 817–824 (2016).
19. K. S. Rao and A. K. Chaudhary, "Investigation of thermal decomposition and stability of energetic 1, 2, 4-triazole derivatives using UV laser based pulsed photoacoustic technique," RSC Adv. **6**, 47646–47654 (2016).
20. F. Yehya, A. K. Chaudhary, D. Srinivas, and K. Muralidharan, "Study of thermal decomposition mechanisms and low-level detection of explosives using pulsed photoacoustic technique," Appl. Phys. B **121**, 193–202 (2015).
21. D. Grischkowsky, S. Keiding, M. van Exter, and C. Fattinger, "Far-infrared time-domain spectroscopy with terahertz beams of dielectrics and semiconductors," J. Opt. Soc. Am. B **7**, 2006–2015 (1990).
22. Y. Sonawane, O. Joshi, and M. Wagh, "Terahertz technology: a boon to tablet analysis," Indian J. Pharm. Sci. **71**, 235–241 (2009).
23. M. Walther, B. Fischer, M. Schall, H. Helm, and P. Jepsen, "Far-infrared vibrational spectra of all-trans, 9-cis and 13-cis retinal measured by THz time-domain spectroscopy," Chem. Phys. Lett. **332**, 389–395 (2000).
24. J. Barber, D. E. Hooks, D. J. Funk, R. D. Averitt, A. J. Taylor, and D. Babikov, "Temperature-dependent far-infrared spectra of single crystals of high explosives using terahertz time-domain spectroscopy," J. Phys. Chem. A **109**, 3501–3505 (2005).
25. I. Abid, W. Chen, J. Yuan, A. Bohloul, S. Najmaei, C. Avendano, R. Péchou, A. Mlayah, and J. Lou, "Temperature-dependent plasmon-exciton interactions in hybrid Au/$MoSe_2$ nanostructures," ACS Photon. **4**, 1653–1660 (2017).
26. T. Trzcinski, N. Palka, and M. Szustakowski, "THz spectroscopy of explosive-related simulants and oxidizers," Bull. Pol. Acad. Sci. Tech. Sci. **59**(4), 445–447 (2012).
27. K. Tanaka, H. Hirori, and M. Nagai, "THz nonlinear spectroscopy of solids," IEEE Trans. Terahertz Sci. Technol. **1**, 301–312 (2011).
28. M. A. Jarzembski, M. L. Norman, K. A. Fuller, V. Srivastava, and D. R. Cutten, "Complex refractive index of ammonium nitrate in the 2–20-μm spectral range," Appl. Opt. **42**, 922–930 (2003).
29. A. K. Chaudhary, A. M. Rudra, P. Kumbhakar, and G. C. Bhar, "Generation of coherent tunable deep UV radiation for detection and absorption studies of explosives RDX and TNT," J. Appl. Spectrosc. **74**, 571–577 (2007).
30. R. Feng, W. Li, Q. Zhou, K. Mu, L. Zhang, and C. Zhang, "Terahertz spectroscopic investigations of explosives and the related compounds," Proc. SPIE **7158**, 71580W (2009).
31. E. Brunol, F. Berger, M. Fromm, and R. Planade, "Detection of dimethyl methylphosphonate (DMMP) by tin dioxide-based gas sensor: response curve and understanding of the reactional mechanism," Sens. Actuators B Chem. **120**, 35–41 (2006).
32. D. G. Allis, J. A. Zeitler, P. F. Taday, and T. M. Korter, "Theoretical analysis of the solid-state terahertz spectrum of the high explosive RDX," Chem. Phys. Lett. **463**, 84–89 (2008).
33. G. Winnewisser, "Spectroscopy in the terahertz region," Vibr. Spectrosc. **8**, 241–253 (1995).
34. Y. C. Shen, P. C. Upadhya, E. H. Linfield, and A. G. Davies, "Temperature-dependent low-frequency vibrational spectra of purine and adenine," Appl. Phys. Lett. **82**, 2350–2352 (2003).
35. M. Hangyo, T. Nagashima, and S. Nashima, "Spectroscopy by pulsed terahertz radiation," Meas. Sci. Technol. **13**, 1727–1738 (2002).
36. A. K. Azad, V. H. Whitley, K. E. Brown, T. Ahmed, C. J. Sorensen, and D. S. Moore, "Temperature dependent terahertz properties of energetic materials," Proc. SPIE **9856**, 98560W (2016).
37. B. M. Fischer, H. Helm, and P. U. Jepsen, "Chemical recognition with broadband THZ spectroscopy," Proc. IEEE **95**, 1592–1604 (2007).
38. J. F. Federici, B. Schulkin, F. Huang, D. Gary, R. Barat, F. Oliveira, and D. Zimdars, "THz imaging and sensing for security applications—explosives, weapons and drugs," Semicond. Sci. Technol. **20**, S266–S280 (2005).
39. W. H. Fan, A. Burnett, P. C. Upadhya, J. Cunningham, E. H. Linfield, and A. G. Davies, "Far-infrared spectroscopic characterization of explosives for security applications using broadband terahertz time-domain spectroscopy," Appl. Spectrosc. **61**, 638–643 (2007).

40. Y. C. Shen, T. Lo, P. F. Taday, B. E. Cole, W. R. Tribe, and M. C. Kemp, "Detection and identification of explosives using terahertz pulsed spectroscopic imaging," Appl. Phys. Lett. **86**, 241116 (2005).
41. R. T. Hall, D. Vrabec, and J. M. Dowling, "A high-resolution, far infrared double-beam lamellar grating interferometer," Appl. Opt. **5**, 1147–1158 (1966).
42. A. Sengupta, A. Bandyopadhyay, J. F. Federici, and R. B. Barat, "Study of morphological effects on terahertz spectra using ammonium nitrate," in *Optical Terahertz Science and Technology* (Optical Society of America, 2005), paper ME6.
43. R. M. Doherty and D. S. Watt, "Relationship between RDX properties and sensitivity," Propell. Explos. Pyrotech. **33**, 4–13 (2008).